

Electrochemical Growth and Charge-Transport Properties of Polyaniline/Poly(styrenesulfonate) Composite Films

Teruhisa Komura,* Kouji Mori, Takahiro Yamaguchi, and Kousin Takahashi

Department of Material Chemistry, Faculty of Engineering, Kanazawa University, 40 Kodatsuno 2-chome, Kanazawa 920

(Received May 27, 1999)

The kinetic parameters of charge transport in composite-modified electrodes were measured as a function of the electrode potential, film thickness, solution pH, and counter ion composition by electrochemical impedance spectroscopy. The impedance characteristics of composite films were analyzed on the basis of the diffusion–migration transport of both holes and protons in the film. Incorporation of the polyanion with the host matrix produced a more compact deposite. A slow growth of the composite film during electropolymerization was ascribed mainly to its low electronic conductivity caused by poor contacts among polyaniline chains. Poly(styrenesulfonic acid) lowered the coupled diffusion coefficient of the charge carriers by a factor of ten. The relationships between the kinetic parameters and the oxidation and protonation levels of polyaniline suggested that the rate of charge transport through the composite film was controlled by electron transport, which occurred probably via interchain electron hopping.

Conjugated polymers such as polyaniline, polypyrrole, and polythiophene have received considerable attention because of possible applications in organic batteries, microelectronic devices, and electrocatalysis. These materials can be electrochemically switched between conducting and insulating states with a substantial change in optical and chemical properties.[1] The rate of change of the polymer oxidation state depends significantly on the nature of both counter ions and co-ions as well as on electronic mobility. To improve the charge-transport properties of conducting polymer films, many investigators are devoting considerable efforts to the preparation of functionalized conducting polymers. A promising method for gaining this goal is to use multicomponent polymer films.

Electrochemical polymerization of an aromatic compound in the presence of a soluble anionic polyelectrolyte (e.g., poly(styrenesulfonate), poly(vinylsulfonate), or poly(vinyl sulfate)) has led to a new kind of multicomponent material with controllable electrical and mechanical properties.[2] Intimate mixing of the positively charged matrix polymer and the charge-compensating polyanion increased the thermal stability and mechanical strength of the film.[2] Since large polyanions entangled with the host matrix cannot move away from the film, the ion-transport properties of conducting-polymer/polyanion composites are expected to differ from those of conducting polymers doped with a small mobile anion.[3] According to the elemental analysis[4] of polypyrrole/polyanion composites in different oxidation states, the composites were predominantly doped with cations during reduction. This observation was confirmed by electrochemical quartz crystal microbalance (EQCM) technique.[2] An ESCA study[5] of polyaniline (PA) similarly reported that poly(styrenesulfonate) (PSS), which interacted strongly with the nitrogen atom of PA, was selectively incorporated with the host matrix. Barbero and others[6] studied the irreversible retention of poly(vinylsulfonate) in PA and the ion exchange of the composite using probe beam deflection and EQCM. Such molecular composites are electronically and ionically conductive over a wide range of their oxidation levels.

Since most of the above applications need fast electrochemical transformation of electroactive polymers, the mixed-conductor properties of molecular composites have attracted a growing interest. However, many points remain unclarified about charge-transport processes in PA/polyanion composites.[1,7] There are two reasons for this: (1) at least three forms of PA are involved in its redox reactions, and (2) most species of different oxidation states are protonated in acid solutions.[7] To understand the mechanism of the coupled electron and ion movement in a PA composite, we thus need to clarify the roles of different oxidation and protonation states in charge transport through the composite film.

The purpose of this paper is to examine the effects of the oxidation and protonation levels of PA/PSS on the kinetic parameters of its redox processes: the redox capacitance, the width of the Warburg region, the conductivity of the film, and the coupled diffusion coefficient of charge carriers. The impedance response of PA/PSS-coated electrodes is interpreted in terms of the diffusion–migration transport of both holes and cations in the film.

Experimental

Preparation of Composite Films. The PA/PSS composites were electrolytically deposited on glassy carbon (GC, 0.071 cm^2 area) from a 0.1 M aniline solution (1 M = 1 mol dm^{-3}) containing 0.5 M poly(4-styrenesulfonic acid) (HPSS) by the potential-cycling method; this acid was prepared from poly(sodium 4-styrenesulfonate) (Aldrich, MW = 7×10^4) using an ion-exchange method. The potential of the working electrode was repetitively cycled between

−0.15 and 0.8 V versus Ag|AgCl at a scan rate of 100 mV s^{-1}. Elemental analysis of PA/PSS: C, 58.40; H, 4.53; N, 8.21; S, 5.67%. The ratio of nitrogen to sulfur showed that one sulfonate anion was incorporated into the composite for every three—four aniline units of PA chains. A linear relationship was observed between the film thickness, measured by scanning electron microscopy, and the voltammetric charge $Q_{0.4}$ passed during the potential scan from −0.2 to 0.4 V (the first oxidation process) in acid solutions. A proportionality constant of 0.34 μm/(mC cm^{-2}) allowed us to estimate a charge density of 0.30 M at 0.4 V. Assuming that the oxidation-charge density at 0.8 V is equal to the sulfonate-group concentration in the film, we estimated this concentration at 0.9 M roughly. A composite film with a selected sulfonate-group/chloride ratio, PA/PSS-Cl, was prepared from a aniline solution containing HPSS and hydrochloric acid in the $-SO_3^-/(-SO_3^- + Cl^-)$ fraction of x.

Apparatus and Procedures. The impedance of PA/PSS-modified GC electrodes was measured at different applied potentials with an NF Electronic Instruments S-5720C frequency-response analyzer coupled to a Hokuto Denko HA-501G potentiostat. Electrochemical experiments were carried out in a two-compartment, three-electrode glass cell under a nitrogen atmosphere. A large Pt gauze (20 cm^2) was used as the counter electrode, and an Ag|AgCl|3.4 M KCl electrode as the reference electrode. In the present paper, all electrode potentials are reported with respect to the Ag|AgCl electrode. Impedance values were determined at five discrete frequencies per decade over the range of 10^4—10^{-3} Hz with a signal amplitude of 7 mV (peak to peak).

The exchange of material between the film and the electrolyte solution during redox reactions was examined with EQCM. A 6 MHz AT-cut quartz crystal with gold electrodes (1.33 cm^2) coated on both sides was used in all experiments. The resonance frequency was measured with a Hokuto Denko HQ-101B QCM controller. For PA/PSS films of different thicknesses, the total frequency change upon deposition of each film showed a linear relationship with the redox charge $Q_{0.4}$. This linearity suggested the rigid layer behavior of the composite film; thus, we concluded that the viscoelastic properties of the film did not influence the measurement.

Results and Discussion

1. Electrodeposition of PA/PSS Composites. First of all, the kinetic features of film deposition during electropolymerization are described. Figure 1 shows a typical current transient measured under potentiostatic conditions in the solutions of different x values. Current–time curves for the potentiostatic polymerization were characterized by a significant increase in current, followed by a gradual fall at long times. The rise in current may correspond to an increase in the surface area of the film, which is due to the growth of a more porous film. No current peak was observed for the film deposition from a HCl solution. Previous studies[7,8] have shown that H_2SO_4 and HCl solutions produce the swollen PA film with a loosely bound open structure. As shown in Fig. 1, the rate of film growth decreases with an increase in x. This result indicates that HPSS produces more compact deposits. Figure 2 shows a plot of the redox charge $Q_{0.4}$ for a PA/PSS film as a function of the electrolysis time. The redox charge for PA/PSS increased up to 30 min, after which it remained nearly constant or decreased gradually. We should notice that the composite film did not grow at all after 30 min. The cessation of film growth arose from a slower electrooxidation of aniline at the surface of a thicker composite film. A slight decrease in $Q_{0.4}$ at long times can be due to the degradation of overoxidized PA. This inference was corroborated by the EQCM frequency response for PA/PSS-modified electrodes held at 0.8 V in aniline-free acid solutions. As shown in Fig. 2, the frequency of the microbalance increases (i.e., the

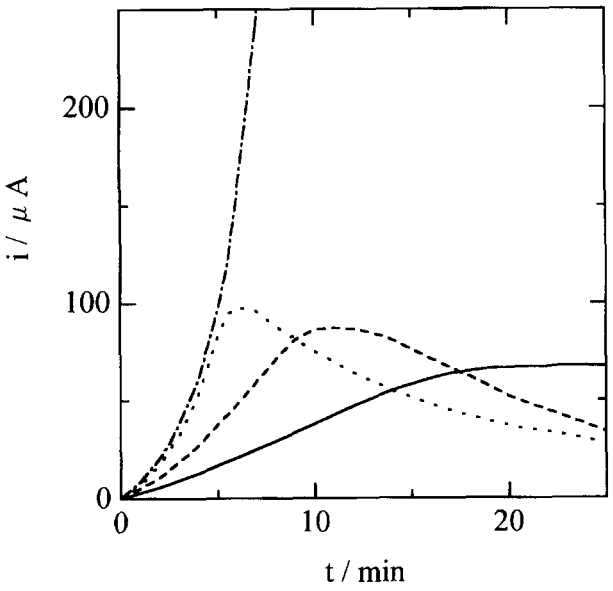

Fig. 1. Potentiostatic current transient for film deposition from 0.1 M aniline solutions of different PSS fractions ($-SO_3^-/(-SO_3^- + Cl^-)$) (—) 1, (- - -) 0.5, (·····) 0.1, and (–·—·–) 0. Electrode potentials were stepped from the rest potential to 0.8 V.

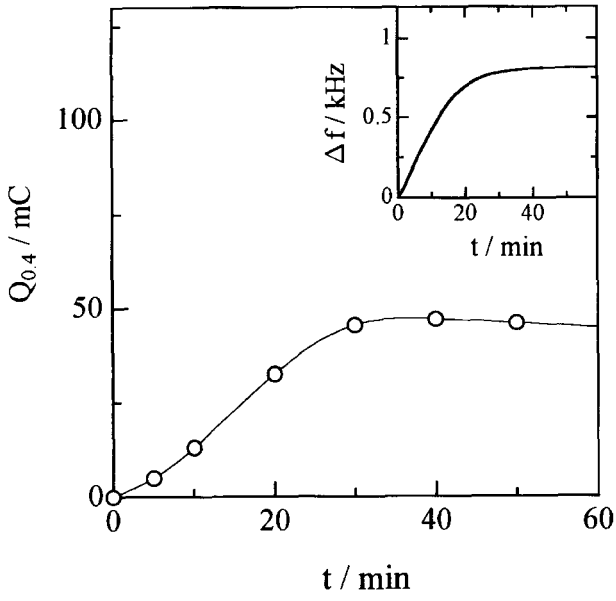

Fig. 2. The charge for the first redox process, $Q_{0.4}$, measured at different stages of electrodeposition. A PA/PSS film was deposited at 0.8 V from a 0.1 M solution of aniline in 0.5 M HPPS. The inset shows the EQCM frequency response for a PA/PSS-modified electrode held at 0.8 V in aniline-free 0.1 M $HClO_4$.

film mass decreases) rapidly with the electrolysis time. The degradation of PA is ascribed to the hydrolysis of quinonoid imine structures formed by overoxidation.[9,10]

The kinetics of film growth was further examined by the potential-cycling method. The redox charge $Q_{0.4}$ increased almost quadratically with the number of potential cycles in the range 0 to 200 cycles. The redox charge obtained at a fixed cycle number depended largely on the anionic composition of the electrolyte solution. Figure 3 shows $\log Q_{0.4}$ versus x plots obtained at different cycle numbers. The redox charge for PA/PSS was less than that for PA/Cl by a factor of 60—80. The rate of growth of a PA/PSS film was equal to 37 $\mu C\,cm^{-2}$ a cycle at a cycle number of 100. The growth rate increased exponentially to about 100 of its original value as x decreased from one to zero.

The foregoing result drives us to the question why the rate of growth of PA/PSS is much slower than that of PA/Cl. Electrochemical thickening of the film is certainly controlled by two processes: electron migration through the film and crystallization on the film surface. Consequently, a large ohmic potential drop across the film diminishes the driving force for electrochemical oxidation of aniline at the film surface. This view can satisfactorily explain the result for the potentiostatic polymerization. Thus, a slow growth of the PA/PSS composite was ascribed to either its low electronic conductivity or its large thickness, or both. This subject will be discussed further in Section 3.

2. Redox Reaction. Oxidation of PA involves at least two kinds of redox reactions:[7] the formation of the radical cation and quinonoid structures. Since the latter form slowly degradates in water, all results reported below relate to the first oxidation process corresponding to the conversion from the reduced state to the half-oxidized state (emeraldine state). Oxidation of a PA film incorporates anions X^- into the film or releases protons from the film to maintain its electroneutrality:

$$-\ddot{N}H- + X^- \rightarrow -\dot{N}H^+-(X^-) + e^- \quad (1)$$

$$-NH_2^+-(X^-) \rightarrow -\dot{N}H^+-(X^-) + H^+ + e^- \quad (2)$$

where –NH– denotes arylamine groups on polymer chains. For ion transport which accompanies the redox switching of PA, there are significant differences among the reported results; however, much evidence has accumulated to show that both anion insertion and proton expulsion occur during oxidation of PA/SO_4 and PA/Cl.[7] The situation in PA/polyanion composites is less complicated, as suggested by a probe beam deflection and EQCM study[6] on the ion exchange of PA/poly(vinylsulfonate); this study indicated that the charge-compensation process at low oxidation levels was dominated by proton exchange at acidic pH values except near zero. A similar EQCM signal was observed for a PA/PSS composite: a decrease in the electrode mass during the anodic potential scan, followed by a mass increase at high oxidation levels. The sulfonate-group concentration in the composite film should be equal to the sum of the concentrations of positively charged amine groups (such as $-NH_2^+-$ and $-\dot{N}H^+-$) and free protons in the film. As a result, it is larger than the concentration of radical cations produced during oxidation up to 0.4 V. Thus, the first redox process for PA/PSS films may not involve any interfacial anion transfer at least in solutions less acidic than 0.5 M HPSS used for electropolymerization. This presumption was supported by the linear dependence of the formal potential (given as the average of anodic and cathodic peak potentials) on the solution pH. Whereas the formal potential of PA/Cl was nearly independent of the pH at pH > 1, that of PA/PSS shifted to more negative values at a rate of 58 mV/pH as the pH increased from 0.5 to 4. This observation suggests that, in acid media, about one proton was released for each electron transferred in the oxidation process.

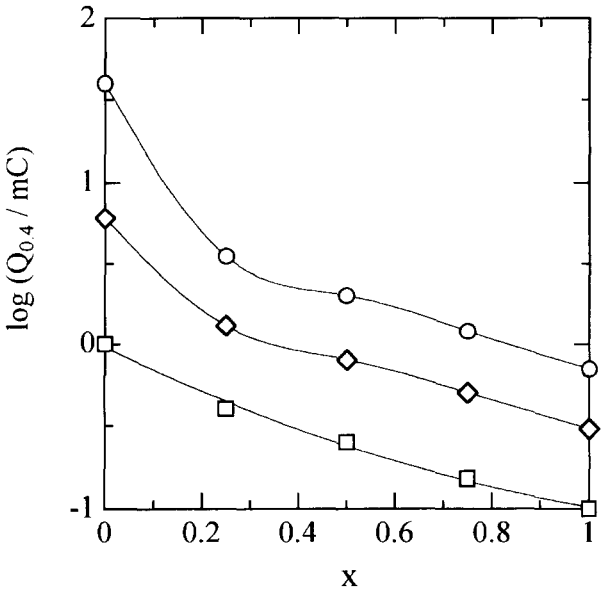

Fig. 3. Plots of $\log Q_{0.4}$ against the PSS fraction x during potential-cycling between −0.15 and 0.8 V. Cycle number: (□) 50, (◇) 100, and (○) 200.

3. Impedance Response. The nature of charge-transport processes in electroactive polymer films is one of the most interesting problems in this research area.[1,7] To understand the notable characteristics of charge transport at PA/PSS-modified electrodes, we have examined their impedance response. When the relaxation times of elemental electrode processes differ much from one another, complex-plane impedance diagrams show different frequency-limited regions of impedance response. Figure 4 represents typical impedance spectra for a PA/PSS-coated GC electrode in 0.5 M PSS solutions; at a constant pH, the same spectra were observed in chloride, sulfate, and perchlorate solutions. The spectra showed a linear 45° region in the high-frequency range and a nearly vertical line in the low-frequency range. Since impedance plots showed wide variation at frequencies higher than 1 kHz, no definite semicircle was discerned in the spectra. These regions of impedance response allowed us to evaluate the charge-transport parameters at the polymer-coated electrode.

High-Frequency Resistance. We describe the ex-

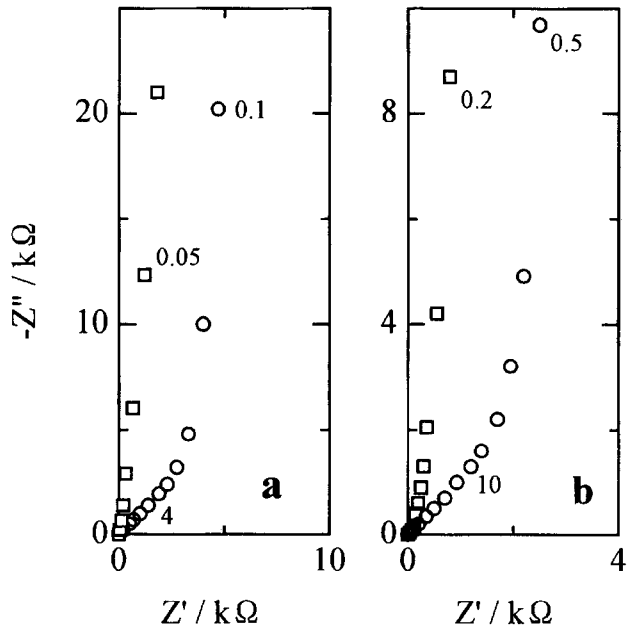

Fig. 4. Typical impedance spectra of a PA/PSS-coated GC electrode in 0.5 M HPSS–NaPSS solutions. (a): (○) applied potential 0 V, (□) 0.3 V; pH 0.8, cycle number = 200. (b): (○) pH 0.8, (□) pH 4; applied potential = 0 V, cycle number = 100. Numerical values in the figure exhibit frequencies in Hz.

trapolated real-axis intercept R_∞ of the 45° line in detail. The high-frequency resistances for PA/PSS films of different thicknesses are plotted against the potential E in Fig. 5. In the potential range 0.2 to 0.4 V, the R_∞ values for the modified electrodes were, within experimental error, the same as those for naked electrodes, which are equal to the solution resistance (20 Ω in 0.5 M HPSS). Thus, the high-frequency resistance of the oxidized film in acid solutions was too small to be measured exactly. At potentials lower than 0.2 V, R_∞ depended largely on the potential and the film thickness. The high-frequency resistance increased rapidly as the potential decreased to 0 V, below which it became nearly constant. The inset in Fig. 5 shows that R_∞ at −0.1 V, corrected for the solution resistance, increases almost linearly with the film thickness. As the pH of the solution was increased, the R_∞-raising potential shifted to more negative values because of the resulting shift in the formal potential. The high-frequency resistance measured at the potential 0.2 V more negative than the voltammetric anodic peak potential increased exponentially with the pH. If the corrected R_∞ is regarded as the film resistance, the foregoing dependences of R_∞ on the potential and the pH are similar to the results reported for a PA/SO_4 film,[11–13] which have shown a broad minimum inside a potential window between the first and second redox processes.

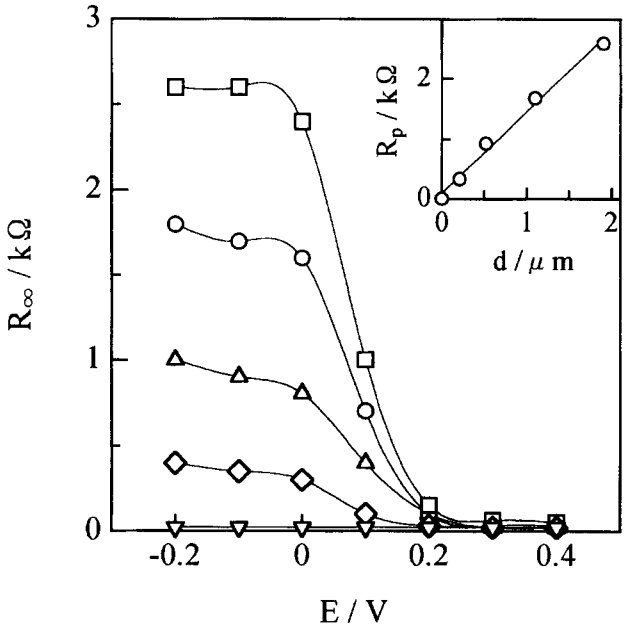

Fig. 5. Plots of high-frequency resistance R_∞ against applied potential at different film thicknesses (▽) 0, (◇) 0.21, (△) 0.52, (○) 1.1, and (□) 1.9 μm. Electrolyte solution: 0.5 M HPSS. The inset shows a linear increase in the film resistance at −0.1 V with increasing film thickness.

The high-frequency resistance varied also with the anionic composition of the film. Figure 6 shows the resistance versus potential plots, measured in 0.3 M (HPSS+HCl), for the films having different $-SO_3^-/Cl^-$ ratios but an equal $Q_{0.4}$ value of 3.1 mC cm^{-2}. The film with a higher $-SO_3^-/Cl^-$ ratio showed a larger resistance in the reduced state. This result can be ascribed in large part to a decrease in the film conductivity caused by the inclusion of PSS. At the above redox charge, the film thickness of PA/PSS was 1.1 μm, whereas that of PA/Cl was 0.76 μm. Assuming the corrected R_∞ was equal to the film resistance, we estimated the conductivity of PA/PSS at 9.8×10^{-6} S cm^{-1} and that of PA/Cl at 7.2×10^{-5} S cm^{-1} at −0.1 V. The latter value is of the same order of

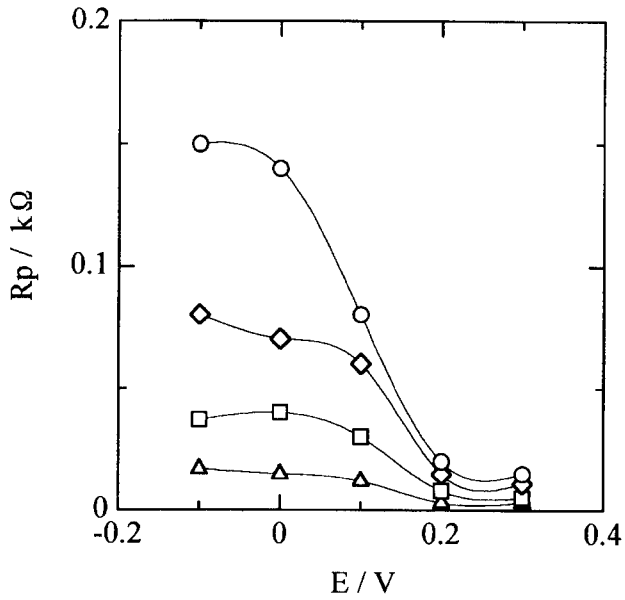

Fig. 6. Film resistance versus applied potential plots at different PSS fractions (△) 0, (□) 0.2, (◇) 0.5, and (○) 1. Films have a $Q_{0.4}$ value of 3.1 mC cm^{-2}. Electrolyte solution: 0.3 M (HPSS+HCl).

magnitude as that reported for the reduced PA/SO_4 film.[14] Our estimate of the film conductivities agrees with the result obtained by Bartlett and Wang;[15] they showed that the resistance of PA/PSS in a pH 5 solution was 170 times as high as the corresponding value for PA/SO_4. Intimate mixing of the host matrix and the charge-compensating polyanion probably diminishes immediate contacts among PA chains. Since good interchain transport is crucial in inducing high electronic conductivity, the slow growth of the composite film can be ascribed mainly to its low conductivity.

However, we are confronted with two difficulties. First, the increase in R_∞ due to polymer reduction conflicts with the change expected for the ionic resistance of the composite film. The ionic resistance may decrease with reduction of PA, because of the proton incorporation into the film:

$$-\dot{N}H^+-(PSS^-)+H^++e^- \rightarrow -\dot{N}H-(PSS^-)(H^+) \quad (3)$$

$$-\ddot{N}H-(PSS^-)(H^+) \rightarrow -NH_2^+-(PSS^-). \quad (4)$$

Second, the change in R_∞ with the anionic composition is inconsistent with that expected for the ionic resistance. The proton incorporation into the reduced PA/PSS may cause its ionic conductivity to be higher than that of the reduced PA/Cl. What has to be noticed is that the protonic equilibrium between the polymer film and the solution involves two steps:[16] (1) proton-partitioning equilibrium affected by the Donnan potential and (2) PA's protonation/deprotonation determined by dissociation constants. Protonation of the anion exchanger PA/Cl with a positive Donnan potential requires a more acidic electrolyte than that of the cation exchanger PA/PSS with a negative Donnan potential does.[16] At a given pH of the solution, thus, the degree of protonation of PA/PSS may be higher than that of PA/Cl. At present, however, very little work on the movement of bound protons is available in the published literature. The changes in R_∞ mentioned above can be related to either interchain proton hopping interrupted by poor PA interchain contacts or proton transport accompanied by intermolecular electron exchange. We were unsuccessful in answering the above two questions definitely.

Redox Capacitance. We will describe the main features of low-frequency characteristics of the impedance response. At low frequencies, charge transport across a thin film is accomplished during one-half cycle of the applied signal; charge-carrier concentrations are almost constant inside the film at each instant. Since the impedance becomes purely capacitive then, the vertical region due to charge saturation is seen on impedance spectra. In this region, the imaginary part of impedance Z'' changes linearly with the reciprocal of the angular frequency ω; thus, the capacitance C_L of the film can be evaluated from

$$dZ''/d\omega^{-1} = 1/C_L. \quad (5)$$

The low-frequency capacitance for the composite film depended on the oxidation level, the film thickness, and the anionic composition. The C_L values obtained for the PA/PSS-coated electrode in a 0.3 M HCl solution are plotted as a function of the potential in Fig. 7. The C_L versus E curves

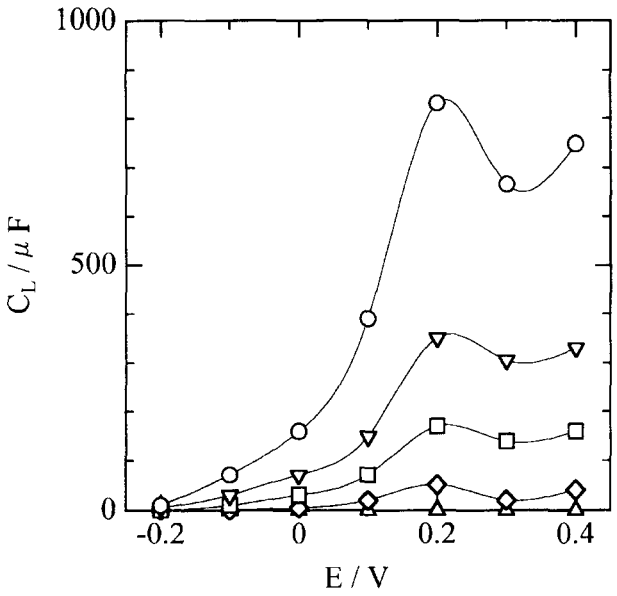

Fig. 7. Low-frequency capacitance versus applied potential plots at different film thicknesses (△) 0, (◇) 0.21, (□) 0.52, (▽) 1.1, and (○) 1.9 μm. Electrolyte solution: 0.3 M HCl.

obtained at different film thicknesses each showed their maxima near 0.2 V, which corresponded to the formal potential. The maximum of C_L increased linearly with the film thickness. The proportionality constant obtained was equal to about 40 F cm^{-3}. Such a large capacitance observed in the partially oxidized state can be attributed to either a high electroactive-site concentration or to the porous nature of the film. The latter causes a large surface effect associated with the double-layer formation. An assumed fibrous structure, however, led us to too fine fibrils (a radius of several nanometers) for the polymer. On the other hand, the anodic charge voltammetrically measured gave as high a charge density as 0.30 M at 0.4 V. This value corresponded to the oxidation of one aniline unit for every 10 aniline units of PA chains.

Assuming the high redox capacity of the composite film, we can relate C_L to the oxidation charge:

$$C_L = dQ/dE, \quad (6)$$

where Q is the charge required to oxidize the fully reduced polymer. The oxidation charge is given by $Q = FAdc_e$, where F is the Faraday constant, A is the electrode area, d is the film thickness, and c_e is the concentration of a hole (i.e., a π bond with the electron missing). Thus, integration of the C_L versus E curve allowed us to estimate c_e from the equation $c_e = (FAd)^{-1}\int C_L dE$. This method gave a c_e value of 0.22 M at 0.4 V for the PA/PSS film. This c_e value was somewhat low compared with that derived from the voltammetric measurement of Q, though C_L should be equivalent to the voltammetric current/scan-rate obtained at slow scan rates for an ideal film electrode.

Since protons participate in the redox reaction of PA, we have to examine the dependence of C_L on the proton concentration in solution. Figure 8 shows C_L versus E plots measured at different pH values of the solution. As the pH

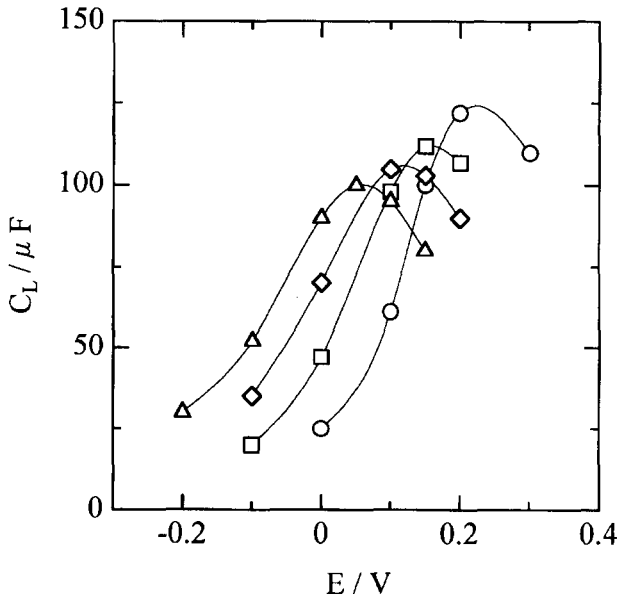

Fig. 8. Low-frequency capacitance versus applied potential curves at different pH values (○) 0.8, (□) 2.1, (◇) 3.0, and (△) 4.1. Electrolyte solution: 0.3 M HCl–NaCl. Film thickness: 0.5 μm.

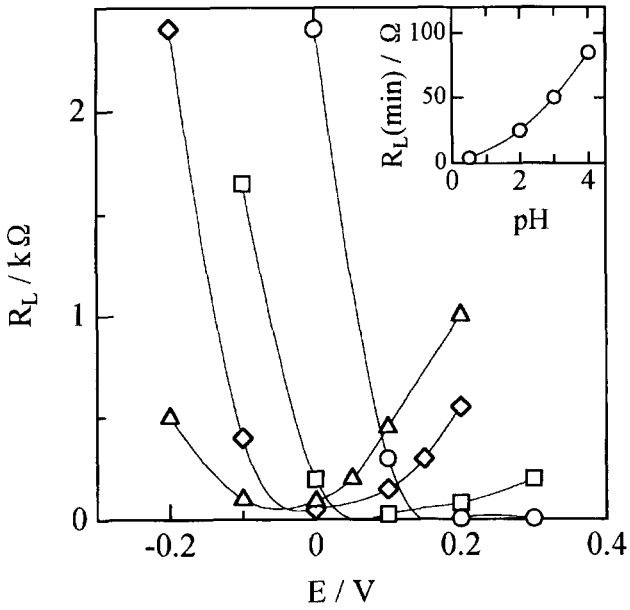

Fig. 9. Plots of the Warburg-region width R_L against applied potential at different pH values (○) 0.8, (□) 2.1, (◇) 3.0, and (△) 4.1. Electrolyte solution: 0.3 M HCl–NaCl. Film thickness: 0.5 μm. The inset shows an exponential increase in the R_L minimum with increasing pH.

increased from 0.5 to 4, the potential of the maximum C_L shifted to more negative values at a rate of about 50 mV/pH. This shift agreed well with the change in the formal potential. The foregoing results suggest that protons penetrate rapidly through the swollen thin film. The maximum of C_L decreased only by 15 percent with the pH increase from 0.5 to 4. Since the oxidation charge showed a similar reduction (10—15%), the gradual decrease in C_L with increasing pH may be due to a slight drop in the electroactive-site concentration.

The Width of the Warburg Region. It should be noted that the width R_L of a linear 45° region (i.e., the Warburg region) corresponding to semi-infinite diffusion varied with the oxidation level of the polymer and the pH of the solution. Figure 9 shows the R_L values determined from complex-plane impedance plots for PA/PSS-coated electrodes. All the R_L versus E plots obtained at different pH values gave typical U-type curves, except the plot measured in 0.3 M HCl; it showed a nearly constant R_L above 0.2 V. As shown in the inset in Fig. 9, the minimum of R_L increases exponentially with the pH. The potential of the minimum R_L shifted to more negative values as the pH increased. At a given potential and pH, R_L increased proportionately with the film thickness in the range 0 to 3 μm.

The width of the Warburg region depended also on the anionic composition of the film. Figure 10 shows R_L versus x plots for the films having different $-SO_3^-/Cl^-$ ratios but an equal $Q_{0.4}$ value of 3.1 mC cm^{-2}. The composite film with a higher $-SO_3^-/Cl^-$ ratio showed a larger R_L in the reduced state. This relation resembles that observed between the anion ratio and the high-frequency resistance.

Charge Transport within Film. We will interpret the impedance response of PA/PSS-coated electrodes according to a uniform conductor model developed by Vorotyntsev.[17,18]

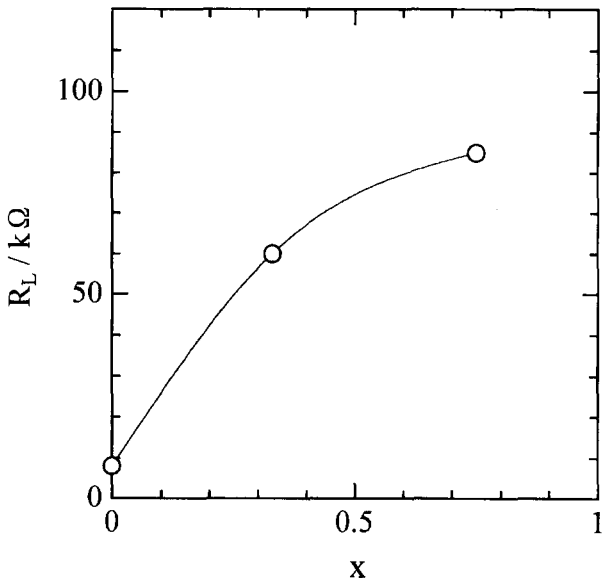

Fig. 10. Plots of the Warburg-region width R_L against the PSS fraction x for films having a $Q_{0.4}$ value of 3.1 mC cm^{-2}. Electrolyte solution: 0.3 M (HPSS+HCl). Applied potential: −0.1 V.

Charge transport within the film is described by the diffusion and the migration of both holes and cations. For the PA/PSS film with an immobile charge, the hole plus cation concentration is reasonably assumed to be equal to the concentration of sulfonate groups. The impedance model developed for another conducting polymer with a polaron/anion couple[17—19] can be applied to the present system, because the presence of immobile charge in the film merely affects the equilibrium-state and transport parameters.

The Faradaic impedance behavior associated with the present model (see Appendix A) is briefly outlined. At high frequencies, the calculated impedance spectrum shows the Warburg region. When the frequency tends to infinity, Eq. A1 reduces to

$$Z(\omega \to \infty) = R_s + R_e + R_i + R_p, \tag{7}$$

where Z is the Faradaic impedance of the electrode, R_s is the solution resistance, R_e is the electronic charge-transfer resistance at the metal|film interface, R_i is the ionic charge-transfer resistance at the film|solution interface, and R_p is the resistance of the bulk film. When the effect of the interfacial capacitance is taken into account, the calculated impedance spectrum gives a semicircle with a diameter of (R_e+R_i) at very high frequencies. At low frequencies, diffusion-migration transport of charge carriers is limited by a finite film thickness; thus, the impedance spectrum shows the vertical region due to charge saturation. The vertical region corresponds electrically to a series combination of the frequency-independent resistance and capacitance. The low-frequency limit of the real part of the impedance is written as

$$Z'(\omega \to 0) = R_s + R_e + R_i + R_p(3t_e t_i)^{-1}, \tag{8}$$

where t_e is the transference number of holes, and t_i is that of cations. Using Eqs. A1, A3, and A4, the low-frequency capacitance is written as

$$C_L = AdF^2(RT)^{-1}c_e c_i(c_e + c_i)^{-1}, \tag{9}$$

where c_i is the concentration of cations inside the film, and the other symbols have their usual meanings. The difference between Z' ($\omega \to 0$) and Z ($\omega \to \infty$) gives the width of the Warburg region as

$$R_L = R_p(1 - 3t_e t_i)(3t_e t_i)^{-1}. \tag{10}$$

Equations 9 and 10 predict the following points. First, the low-frequency capacitance increases proportionately with the film thickness. Second, the capacitance has a maximum at the equal concentrations of holes and cations, that is, at the formal potential. Third, the width of the Warburg region also increases linearly with the film thickness, since the bulk-film resistance is proportional to the film thickness, as shown by Eq. A4. Fourthly, the Warburg region decreases in width to $R_p/3$ as t_e (or t_i) tends to 0.5. Finally, a change in R_L with the oxidation level is determined by the corresponding change in R_p divided by both transference numbers. The main features predicted from the present model are consistent with the experimental results.

As expected from Eq. 10, the ratio of R_p to R_L can give us useful information on transference numbers.[20,21] The ratio is equal to zero in extreme cases of both ion-transport control ($t_e = 1$, $t_i = 0$) and electron-transport control ($t_e = 0$, $t_i = 1$), whereas it is equal to three for mixed control ($t_e = t_i$). The impedance response of PA/PSS films measured in a 0.3 M HCl solution gave an R_p value of 0.05—0.5 kΩ and an R_L value of 5—100 kΩ in the potential range 0 to −0.1 V. The R_p/R_L ratio was obviously very low at potentials below 0.2 V at least. These results make it clear that $t_e \ll t_i$ or $t_e \gg t_i$ at low oxidation levels.

The question which we must consider next is to determine the transport-controlling process. At the two extremes of rate control ($3t_e t_i \ll 1$), Eq. 10 reduces to

$$3R_L = R_p(t_e t_i)^{-1}. \tag{11}$$

Since $R_p(t_e t_i)^{-1}$ is equivalent to the sum of the electronic film resistance R_p/t_e and the ionic film resistance R_p/t_i, the measured R_L enables us to estimate the sum of these resistances. This finding corresponds to the treatment of Albery and Mount,[22] who have proposed a transmission line model in which the electronic and ionic resistances are combined by a distributed capacitance. As shown above, the width of the Warburg region decreased with oxidation of the polymer except for a slight increase at high oxidation levels. The result can reasonably be explained by assuming that $R_p(t_e t_i)^{-1}$ is dominated by electronic transport through the film. This assumption is based on the following experimental result: The change in R_L with the potential was compatible with that expected of the electronic film resistance, whereas it was opposite to that expected of the ionic film resistance. The electronic conductivity of the PA/PSS composite should increase with its oxidation because of an increase in hole concentration. The experimental result above indicates that the ionic film resistance makes a negligible contribution to $R_p(t_e t_i)^{-1}$. From these observations, we can safely state that t_i is considerably larger than t_e.

At the extremes of rate control, the coupled diffusion coefficient D for holes and cations can be estimated. Since the electronic charge carrier and the mobile ion compose a binary electrolyte to retain the local electroneutrality of the film, D is defined by[19]

$$D = D_e D_i(c_e + c_i)(D_e c_e + D_i c_i)^{-1}. \tag{12}$$

where D_e is the diffusion coefficient of holes, and D_i is that of cations. Combining Eqs. A3, A4, 9, 10, and 12, we obtain

$$R_L + R_p = d^2(3DC_L)^{-1}. \tag{13}$$

When $R_L \gg R_p$ (i.e., $t_i \fallingdotseq 0$ or $t_e \fallingdotseq 0$), Eq. 13 reduces to

$$D = d^2(3C_L R_L)^{-1}. \tag{14}$$

This equation allowed us to calculate the coupled diffusion coefficient from the measured values of C_L and R_L. The determined D values are plotted as a function of the potential in Fig. 11. The D versus E plots obtained at different pH values each showed a maximum. The potential of the maximum D shifted to more negative values as the pH increased. As shown in the inset in Fig. 11, the maximum of D decreases exponentially with increasing pH. A similar change in D with the pH was observed for poly(*o*-aminophenol) by Nieto and Tucceri,[23] who considered the charge-transport process controlled by electron motion. To examine a variation in D with the anionic composition, we estimated the coupled diffusion coefficients for the films having different $-SO_3^-/Cl^-$ ratios but an equal $Q_{0.4}$ value of 3 mC cm^{-2}. At a constant

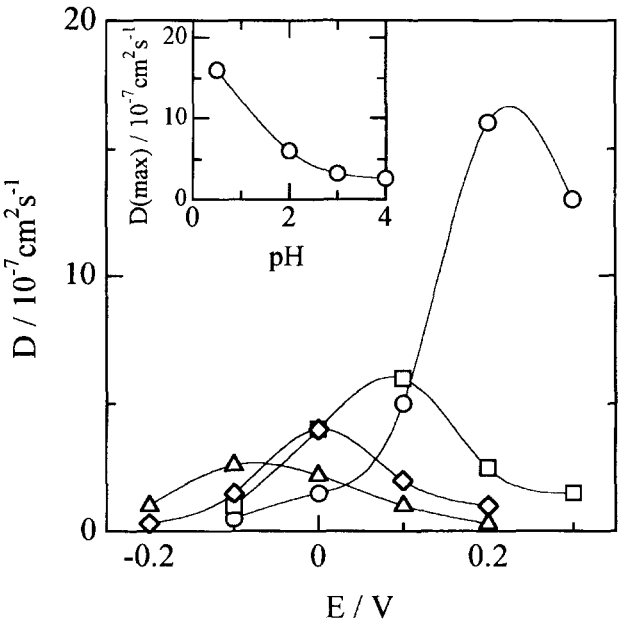

Fig. 11. Coupled diffusion coefficient versus applied potential plots at different pH values (○) 0.8, (□) 2.1, (◇) 3.0, and (△) 4.1. The inset shows an exponential decrease in the D maximum with increasing pH.

redox charge, D was dominated by variations in R_L and d because of no significant change in C_L. The coupled diffusion coefficient decreased gradually with the $-SO_3^-$ fraction from 2×10^{-7} cm^2 s^{-1} for pure PA/Cl to 2×10^{-8} cm^2 s^{-1} for pure PA/PSS at 0.05 V. Incorporation of the polyanion with the host matrix resulted in an appreciable decrease in D.

Since an expression of $t_i \gg t_e$ may require D_i to be larger than D_e, the individual diffusion coefficients are discussed below. Substitution of Eq. A3 in Eq. 12 leads to

$$D = D_i t_e + D_e t_i. \quad (15)$$

At the extreme of electron-transport control ($t_e = 0$, $t_i = 1$), we may identify D with D_e. Although D values ranging from 10^{-3} to 10^{-11} cm^2 s^{-1} have been reported for mobile-anion-doped PA films, published data on the individual diffusion coefficients are limited. For PA/Cl, PA/SO_4, and PA/ClO_4, Deslouis and co-workers[24] reported ion diffusion coefficients of the order of 10^{-6} cm^2 s^{-1} and electron diffusion coefficients ranging from 10^{-5} to 10^{-3} cm^2 s^{-1}. This ion diffusion coefficient agrees with that derived from chronoamperometry by Lacroix for PA/SO_4,[25] whereas it differs considerably from that of the order of 10^{-10} cm^2 s^{-1} obtained by Rudzinski for PA/Cl.[26] The ion diffusion coefficient for proton-doped PA/PSS can be larger than that for anion-doped PA/Cl, since protons may move within the film via a Grotthus-type process. Disregarding the contribution from the quinonoid structure, we estimated c_i in PA/PSS from the difference between the sulfonate-group and hole concentrations. The oxidation charge versus potential plot measured in a 0.3 M HCl solution gave $c_e = 0.01$ M and $c_i = 0.89$ M at -0.1 V, and $c_e = 0.02$ M and $c_i = 0.88$ M at 0 V. The concentration of free protons may be smaller than the estimated c_i values. Previous studies[26,27] have, however, indicated that the fully protonated form of the reduced PA is obtained in strong acid media of pH<1. For instance, a pK_a value of 1.5 was reported by Rudzinski and co-workers for the reduced polymer.[26] The above observations indicate that t_i is considerably larger than t_e at low oxidation levels unless D_i is smaller than D_e.

At the extreme of electron-transport control, the measured diffusion coefficients are attributed to intrachain electron transport or interchain electron hopping. The observed increase in D with decreasing $-SO_3^-$ fraction is interpreted as a reduction in the distance between two adjacent PA chains. Thus, it is reasonable to presume that the rate of electron transport in the composite film is controlled by interchain electron hopping. According to a microscopic model for electron hopping between adjacent redox sites,[1,7] the electron diffusion coefficient can depend on the following quantities: the rate constant of intermolecular electron transfer, the mean distance between two adjacent redox sites, the interaction parameter between redox sites, and the ratio of reduced-site to oxidized-site concentrations. A variation in D with the oxidation level has sometimes been related to the mutual interaction between electroactive sites.[1,7] This is too complicated a subject to be treated here in detail. The strength of the interaction is proportional to the total electroactive-site concentration.[1] This concentration in PA/PSS decreased only by 10—15 percent with an increase in pH from 0.5 to 4; thus, the interaction parameter in the composite film can loosely be related to an electron-transport process. Unlike this, the ratio of reduced-site to oxidized-site concentrations varies directly with the oxidation level of the polymer. The probability of electron hopping from a reduced site to an oxidized site has a maximum at their equal concentrations. This dependence on the concentrations satisfactorily explains the D versus E curves observed for the composite film. The change in D with the pH, on the other hand, can be related to the pH dependence of the rate constant of intermolecular electron transfer. According to previous studies,[7,11—13] the protonated salt form of the half-oxidized polymer (i.e., the radical cation structure) is electronically conductive, but its unprotonated base form (a combination of quinonoid and benzenoid structures) is insulating: the deprotonation is written as

$$-\dot{N}H^+-C_6H_4-\ddot{N}H-C_6H_4-\dot{N}H^+-C_6H_4-\ddot{N}H-C_6H_4- \longrightarrow$$
$$-\ddot{N}=C_6H_4=\ddot{N}-C_6H_4-\ddot{N}H-C_6H_4-\ddot{N}H-C_6H_4- + 2H^+. \quad (16)$$

On transfering from the reduced to oxidized sites, consequently, electrons will hop from the $-NH_2^+-$ to $-\dot{N}H^+-$ groups. Thus, deprotonation of the polymer should diminish the rate constant of intermolecular electron transfer. The same conclusion is derived from interchain electron hopping accompanied by intermolecular proton exchange (inferred from Eq. 2). A rise in the solution pH, therefore, lowers the electron diffusion coefficient.

Conclusions

The impedance response of the PA/PSS film is reasonably

explained on the diffusion–migration transport of both holes and protons. The main results obtained are shown below.

1. A slow growth of PA/PSS, a compact film, during electropolymerization is ascribed mainly to its low electronic conductivity caused by poor interchain contacts.
2. Upon oxidation, the composite film releases about one proton for each electron transferred in the oxidation process.
3. The low-frequency capacitance shows a maximum at the formal potential. It decreases slightly with the solution pH, because of a reduction in the electroactive-site concentration.
4. A decrease in R_L with oxidation of PA indicates that t_i is considerably larger than t_e at low oxidation levels.
5. Incorporation of the polyanion with the host matrix lowers the coupled diffusion coefficient, because of poor interchain contacts in the film produced.
6. Changes in D with the oxidation and protonation levels of PA suggest that the rate of charge transport within the composite film is controlled by electron transport, which occurs probably via interchain electron hopping.

Appendix A

According to the theoretical impedance model,[17,18] the Faradaic impedance of the conducting-polymer-coated electrode can be expressed by

$$Z = R_s + R_e + R_i + R_p(4t_e t_i)^{-1} [\nu^{-1}\coth\nu + (t_e - t_i)^2 \nu^{-1}\tanh\nu]. \quad \text{(A1)}$$

The dimensionless frequency ν is defined by

$$\nu^2 = (j\omega d^2/4)(D_e c_e + D_i c_i)[D_e D_i (c_e + c_i)]^{-1}, \quad \text{(A2)}$$

where j is the imaginary unit. Equation A1 is the same with the impedance expressions derived by Vorotyntsev,[17,18] except for transport parameters. The transference numbers are here defined by

$$t_e = D_e c_e (D_e c_e + D_i c_i)^{-1}, \quad t_i = D_i c_i (D_e c_e + D_i c_i)^{-1}. \quad \text{(A3)}$$

Being a parallel combination of the electronic and ionic resistances, the bulk-film resistance is given by

$$R_p = dRTA^{-1}F^{-2}(D_e c_e + D_i c_i)^{-1}. \quad \text{(A4)}$$

References

1 M. E. G. Lyons, in "Electroactive Polymer Electrochemistry," ed by M. E. G. Lyons, Plenum Press, New York (1994), Part 1, p. 37.

2 C. K. Baker, Y. J. Qiu, and J. R. Reynolds, *J. Phys. Chem.*, **95**, 4446 (1991).

3 X. Ren and P. G. Pickup, *J. Phys. Chem.*, **97**, 5356 (1993).

4 T. Shimizu, A. Ohtani, T. Iyoda, and K. Honda, *J. Electroanal. Chem.*, **224**, 123 (1987).

5 K. Hyodo, N. Kobayashi, and Y. Kagami, *Electrochim. Acta*, **36**, 799 (1991).

6 C. Barbero, M. C. Miras, O. Haas, and R. Kötz, *J. Electrochem. Soc.*, **144**, 4170 (1997).

7 G. Inzelt, in "Electroanalytical Chemistry," ed by A. J. Bard, Marcel Dekker, New York (1994), Vol. 18, p. 89.

8 P. Nunziante and G. Pistoia, *Electrochim. Acta*, **34**, 223 (1989).

9 L. Arsov, W. Plieth, and G. Koßmehl, *J. Solid State Electrochem.*, **2**, 355 (1998).

10 D. E. Stilwell and S. M. Park, *J. Electrochem. Soc.*, **135**, 2497 (1988).

11 W. W. Focke, G. E. Wnek, and Y. Wei, *J. Phys. Chem.*, **91**, 5813 (1987).

12 P. M. McManus, R. J. Cushman, and S. C. Yang, *J. Phys. Chem.*, **91**, 744 (1987).

13 C. Zhang, B. Yao, J. Huang, and X. Zhou, *J. Electroanal. Chem.*, **440**, 35 (1997).

14 K. Roßberg, G. Paasch, L. Dunsch, and S. Ludwig, *J. Electroanal. Chem.*, **443**, 49 (1998).

15 P. N. Bartlett and J. H. Wang, *J. Chem. Soc., Faraday Trans.*, **92**, 4137 (1996).

16 K. Doblhofer and M. Vorotyntsev, in "Electroactive Polymer Electrochemistry," ed by M. E. G. Lyons, Plenum Press, New York (1994), Part 1, p. 410.

17 M. A. Vorotyntsev, J. P. Badiali, and E. Vieil, *Electrochim. Acta*, **41**, 1375 (1996).

18 M. A. Vorotyntsev, L. I. Daikhin, and M. D. Levi, *J. Electroanal. Chem.*, **364**, 37 (1994).

19 R. P. Buck, M. B. Mádáras, and R. Mäckel, *J. Electroanal. Chem.*, **362**, 33 (1993).

20 M. F. Mathias and O. Haas, *J. Phys. Chem.*, **97**, 9217 (1993).

21 M. F. Mathias and O. Haas, *J. Phys. Chem.*, **96**, 3174 (1992).

22 W. J. Albery and A. R. Mount, in "Electroactive Polymer Electrochemistry," ed by M. E. G. Lyons, Plenum Press, New York and London (1994), Part 1, p. 443.

23 F. J. Rodriguez Nieto and R. I. Tucceri, *J. Electroanal. Chem.*, **416**, 1 (1996).

24 A. Benyaich, C. Deslouis, T. Moustafid, M. Musiani, and B. Tribollet, *Electrochim. Acta*, **41**, 1781 (1996).

25 J. C. Lacroix, K. K. Kanazawa, and A. Diaz, *J. Electrochem. Soc.*, **136**, 1308 (1989).

26 W. E. Rudzinski, L. Lozano, and M. Walker, *J. Electrochem. Soc.*, **137**, 3132 (1990).

27 Z. Ping, G. E. Nauer, H. Neugebauer, and J. Theiner, *J. Electroanal. Chem.*, **420**, 301 (1997).